Modulation of cosmic ray ground-level enhancements by solar wind stream interface: a case study

Olakunle Ogunjobi[1] and William Tafon Sivla[2]

[1]Department of Physics and Astronomy, University of Calgary, Canada
[2]Department of Physics and Astronomy, University of Nigeria Nsukka, Nigeria

Correspondence: Olakunle Ogunjobi (olakunle.ogunjobi@ucalgary.ca)

Abstract. Ground Level Enhancements (GLEs) provide crucial insights into the acceleration and transport of solar energetic particles (SEPs). We present a comprehensive analysis of GLE 72, which occurred on 10 September 2017, coinciding with a solar wind stream interaction region (SIR) impacting Earth's magnetosphere. By combining multi-station neutron monitor observations with a focused transport model constrained by solar wind data, we investigate how the SIR modulates the observed GLE pulse shape. Our analysis reveals that the turbulent magnetic field within the SIR significantly enhances pitch-angle scattering rates, with the diffusion coefficient increasing by up to 200% during the 6-hour SIR crossing. This leads to a 60% increase in the particle mean free path across the SIR. Our model successfully reproduces the observed gradual rise phase (>8 hours) and prolonged decay, demonstrating that even moderate interplanetary disturbances can substantially alter SEP transport conditions. Our results challenge the traditional impulsive-gradual classification of GLEs, highlighting the need to consider interplanetary transport effects when interpreting these events. The findings of this study highlight the importance of integrating multi-point observations and advanced modeling to disentangle particle acceleration and transport processes in the complex medium of solar wind.

1 Introduction

Ground level enhancements (GLEs) offer a useful measure of the most intense solar energetic particle (SEP) events through detecting secondary particle shower signatures with ground-based neutron monitor stations (Väisänen et al., 2021). GLEs highlight primary protons accelerated up to several GeV at the Sun when a fraction channel along field lines intersecting Earth's magnetic field. The transient intensity enhancement depends on the SEP spectral shape but typically ranges from 10-100% above background galactic cosmic ray fluxes. Since the first registered GLE in 1942, ground monitors across the globe have detected over seven scores of events correlated with intense flares and fast coronal mass ejections (Canfield et al., 1999; **?**).

Ground Level Enhancements (GLEs) are often characterized as either "impulsive" or "gradual" based on their temporal profiles, particularly their rise and decay times. Impulsive events are typically associated with solar flares and exhibit rapid rises and shorter durations, while gradual events are often linked to CME-driven shocks and show slower rises and longer durations. However, this classification can be complicated by interplanetary transport effects.

Figure 1 shows the distribution of rise and decay times for a sample of 35 GLEs observed between 1956 and 2017. The rise time (τ_r) is defined as the time from event onset to maximum intensity, while the decay time (τ_d) is the time for the intensity to decrease from its maximum to half-maximum value. As evident from the figure, there is considerable overlap between the traditionally classified "impulsive" and "gradual" events, highlighting the challenge in definitively categorizing GLEs based solely on their temporal profiles. Our analysis of GLE 72 ($\tau_r \approx 2$ hours, $\tau_d \approx 14$ hours) places it in a region of overlap between impulsive and gradual classifications. This underscores the importance of considering interplanetary transport effects, such as those induced by stream interaction regions, in interpreting GLE temporal profiles.

Temporal intensity profiles or pulse shapes measurable during GLE events provide insight into the particle acceleration mechanisms and interplanetary transport processes shaping the spectra (Reames, 1999; Cane et al., 2010). Short, impulsive enhancements suggest rapid acceleration by solar flares while shocks driven by fast CMEs produce more gradual, long duration events (Miroshnichenko and Gan, 2012). However, the actual shape of GLE profiles includes considerable modulation during interplanetary propagation, complicating simple classification schemes based solely on pulse characteristics. This author has previously contributed to previous work (Strauss et al. (2017)), hereafter referred to as Paper 1), which quantified rise and decay times for multiple GLEs, and discovered a remarkable universal linear relationship where $\tau_d \approx 3\tau_r$ spanned short, impulsive events to long-term, gradual ones. This suggests frequent, strong pitch angle scattering leading to near-isotropic particle distributions may dominate, obscuring the original injection profile details. Thus, the pulse shape alone provides limited insight about intrinsic acceleration processes.

A key factor complicating GLE observations are transient disturbances propagating through the solar wind, such as stream interaction regions (SIRs) formed from the complex interaction between slow (400 km/s) and fast (800 km/s) solar wind flows (Gosling and Pizzo, 1999; Richardson, 2018). The compressed plasma and magnetic fields within SI s drive substantially enhanced magnetospheric convection (Tao et al., 2005), which can modulate loss processes acting on propagating energetic particles; through mechanisms like magnetopause shadowing, wave-particle interactions, and microburst precipitation (Morley et al., 2010; Ogunjobi et al., 2014; Ogunjobi et al., 2017). Furthermore, pitch angle scattering rates likely fluctuate in response to whistler waves excited by anisotropic distributions, actively altering transport conditions tied to field lines mapping to the radiation belts. Local shocks and turbulence, according to previous work, offer additional acceleration avenues (Li et al., 2003).

Thus, SI dynamics require consideration when interpreting SEP profiles detected at Earth (Richardson and Cane, 1995; Huttunen et al., 2005). In this study, we employ a multi-station analysis paired with transport modeling constrained by actual solar wind conditions to assess fortuitous SI impacts on the GLE 72 observation. More broadly, we explore limitations of intensity-time characteristics for definitively classifying SEP events when the interplanetary medium actively shapes the particle distributions detected at Earth's bow shock nose (BSN). The work specifically, however, tests if transient effects associated with the SI alone can force strong scattering sufficient to mask the intrinsic SEP profile even for a moderate intensity GLE event.

2 Observations

2.1 Neutron monitor: Case study of GLE 72

We utilize observations from the global neutron monitor network to quantify intensities and characterize the temporal profile of GLE 72 which occurred on 10 September 2017. The GLE 72 event was analyzed, in separate studies, by Copeland et al. (2018), who noted very increases above atmospheric secondary particle backgrounds at commercial aircraft altitudes. A collection detailing the occurrence times and intensities of historical GLEs is provided through the cosmic ray group at Izmiran (ftp://cr0.izmiran.rssi.ru/COSRAY!/FTP_GLE/) as well as real-time monitoring at the University of Oulu (https://gle.oulu.fi/). An additional database collating measurements across different stations was described by Moraal and Caballero-Lopez (2014). We incorporate observations spanning > 1 cutoff rigidities, including polar stations such as Dome (DOME), Forth Smith (FSMT), Jang Bogo (JBGO), South Pole (SOPB), Terre Adelie (TERA) and Thule (THUL); lower latitude sites in Rome/Athens (ATHN), alongside the equatorial Mexico City station (MXCO). In total, quality-controlled count rates are gathered from eight independent monitors. The multi-station coverage allows constraining both the spectral and temporal characteristics of the GLE.

GLE 72 normalized count rate profiles are shown in figure 2 for the selected neutron monitor stations as discussed in Section 2. Multi-station analysis confirms the moderate intensity of the event, peaking between 20-30% above background across multiple stations. In particular, the prolonged rise time at South Pole is noteworthy, which does not reach its maximum until nearly 2 hours after injection. This contrasts with the typical sub-hour onsets expected for relativistic protons if scattering is weak (Bieber et al., 2002). Further, Terre Adelie shows intensity dropouts preceding the main event that resemble loss cone signatures (Rawat et al., 2006). According to Morley et al. (2010), this may be the result of transient magnetospheric effects caused by SI compressions and convection enhancements. In spite of modest scattering strength, an impulsive injection produces intensity peaks more rapidly than measured. Nevertheless, the sub-Alfvénic interval established downstream of the reverse shock within the stream interaction provides suitable conditions for driving strong turbulence through firehoses and other kinetic instability phenomena. Therefore, modeling the transport without taking into account propagation upstream through the identified stream interface may result in poor agreement with the observed time profiles. By modeling the transport in detail, we can obtain the expected diffusion coefficients and scattering mean free paths.

2.2 OMNI: stream interface arrival during GLE 72

The SI arrival timing is observed using solar wind plasma measurements from the OMNI database. The OMNI dataset, sourced from http://omniweb.gsfc.nasa.gov, is generated by integrating and cross-normalizing field and plasma measurements acquired at the BSN from various contributing spacecraft. This process, as outlined by King and Papitashvili (2005), involves the interspersion of these measurements after thorough cross-normalization. Parameters including proton density, velocity, and dynamic pressure are assessed using the SI identification criteria defined in prior studies (Jian et al., 2006; Morley et al., 2010; Ogunjobi et al., 2014; Borovsky and Denton, 2016). We scan data $\pm$ 3 days across 10 September 2017 to isolate the stream interaction

region preceding GLE 72. The exact SI arrival at Earth established by sharp velocity gradients and density drops then serves as the alignment point for analysis.

Figure 3 shows some of the plasma parameters that were detected by the OMNI database. A characteristic signature of SI s can be seen in the top three panels (3 (a-c)) which show compressed slow solar wind fields and steepening flows as they reach fast wind (Burlaga, 1974; Jian et al., 2006). SI onset is indicated by the vertical line (a region that delineates compressed fast solar wind from compressed slow solar wind). As SI arrived, we observed enhanced magnetospheric convection (3 (a)). As a result, the magnetopause has moved inward from its standoff location, thus causing ring current decay (3 (b)). There is a significant increase in densities over 12 hours as a result of this compression (3 (c)), while bulk velocities are rapidly shifted from 350 km/s to 650 km/s (3 (d)) as a result of this compression. The density increase closely follows the empirical relation $\rho \approx VSW - 4.4$ identified for stream interfaces. Correspondingly, the dynamic pressures in panel (3 (e)) strengthened by a factor of ≈ 3.5 from September 10th through 11th. The Alfvén Mach number in (3 (f)) breaks below unity within the stream interface between September 9th and September 10th, which is a critical change in the stream's dynamics. At this point, a transition has taken place where the forward shock boundary has transitioned into a reverse shock structure. Embedded sub-Alfvenic flows support the generation of fast/whistler mode turbulence based on kinetic instabilities operating at length scales smaller than the inertial length of ions. There is evidence that the firehose instability is caused by density gradients associated with velocity shears (Kabin et al., 2007). As a result, scattering power can be concentrated in directions near-parallel to the mean field. Through the stream interface geophysical parameters demonstrate a 28% compression of the magnetic field intensity, causing particle trajectory to be further altered by the mirror force.

It is expected that the subsequent injection of the SEP event, commencing on September 10th, will encounter streams that have decelerated from earlier coronal hole streams. During the sub-Alfvénic portion of the SI , pitch angle scattering rates started increasing, sustaining near-isotropic distributions within the sub-Alfvénic portion. In other words, instead of the highly anisotropic beam profile that would have been expected for impulsive flare acceleration, the observed gradual intensities were produced instead.In addition to local shock acceleration (Li et al., 2003), some contributions from the reverse shock of the SI (rotation of solar wind azimuthal velocity from negative to positive (3 (g)) are likely to have occurred. There is, however, evidence that the dominant process persisting the GLE 72 SEP rise and modifying intensities is a consequence of transient effects propagating through the SI structure.

In the presence of sub-Alfvénic flows, whistler turbulence can be generated at the stream interface, which indicates that the SI is capable of producing strong pitch angle scattering. The effects of transient dynamics across compressions are quantified using a Monte Carlo model adapted to transient dynamics.

2.3 Quantification of turbulence levels

The magnetic field data from the OMNI database were analyzed in detail in order to provide concrete evidence for the levels of turbulence discussed in this study. Specifically, we examined the 24-hour intervals surrounding September 9, 10, and 11,

2017, before, during, and after GLE 72. In order to quantify the turbulence, we used two complementary techniques: the Power Spectral Distributions (PSDs) analysis (Goldstein et al., 1995; Leamon et al., 1998) and the Structure Functions (SFs) analysis (Burlaga and Klein, 1986; Horbury and Balogh, 1997). PSDs provide information about the distribution of fluctuation energy across different frequencies, while (SFs) provide insight into turbulence's spatial scales. There is considerable evidence to support the usefulness of both techniques in the analysis of solar wind turbulence, which can be found elsewhere (Bruno and Carbone, 2013).

Figure **??** shows the results of our analysis. For each of the three interest periods, the top panel displays the PSDs of the magnetic field magnitude. We observe a clear enhancement in the power at all frequencies during the GLE event (September 10), particularly in the range of 10^{-4} to 10^{-2} Hz, corresponding to spatial scales of approximately 10^4 to 10^6 km. This increase in power indicates heightened turbulence levels during the event. The bottom panel of Figure **??** shows the second-order structure function of the magnetic field magnitude. The structure function, $SF_2(\tau)$, is defined as:

$$SF_2(\tau) = \langle |B(t+\tau) - B(t)|^2 \rangle \tag{1}$$

where $B(t)$ is the magnetic field magnitude at time t, τ is the time lag, and $\langle ... \rangle$ denotes an ensemble average. The structure function shows a steeper slope during the GLE event, indicating a more developed turbulent cascade.

We also calculated the correlation length, L_c, defined as the integral of the normalized autocorrelation function:

$$L_c = \int_0^\infty \frac{\langle B(t)B(t+\tau) \rangle}{\langle B^2(t) \rangle} d\tau \tag{2}$$

The correlation lengths for the three periods are:

- September 9 (pre-event): $L_c = 1.2 \times 10^6$ km
- September 10 (during event): $L_c = 8.5 \times 10^5$ km
- September 11 (post-event): $L_c = 1.4 \times 10^6$ km

During the GLE event, a shorter correlation length further confirms the presence of enhanced turbulence, as it indicates a more rapidly fluctuating magnetic field. As a result of these quantitative analyses, we have strong evidence supporting our interpretations of particle transport processes discussed herein.

3 Model

3.1 Focused transport equation

In this study, we solve the focused transport equation (FTE) to model the propagation of solar energetic particles (SEPs) through the interplanetary medium. The FTE, first derived by Roelof (1969) and further developed by Ruffolo (1995), describes the evolution of the particle phase space density $f(z, \mu, t)$ along a magnetic field line. Here, z is the distance along the field line, μ is the cosine of the particle's pitch angle, and t is time. Here, our model uses the following form of FTE:

$$\frac{\partial f}{\partial t} + \mu v \frac{\partial f}{\partial z} + \frac{1-\mu^2}{2L} v \frac{\partial f}{\partial \mu} = \frac{\partial}{\partial \mu}\left(D_{\mu\mu} \frac{\partial f}{\partial \mu} \right) \tag{3}$$

where v is the particle speed, L is the focusing length defined as $L^{-1} = -B^{-1}(\partial B/\partial z)$ with B being the magnetic field strength, and $D_{\mu\mu}$ is the pitch-angle diffusion coefficient.

The terms on the left-hand side of Equation 3 represent, from left to right:

- Temporal evolution of the distribution function
- Spatial convection along the magnetic field
- Pitch-angle focusing due to the diverging magnetic field

The right-hand side describes pitch-angle scattering due to magnetic fluctuations. We parametrize the pitch-angle diffusion coefficient following Dröge et al. (2010):

$$D_{\mu\mu}(z, \mu) = D_0(z)(1-\mu^2)(|\mu|^{q-1} + H) \tag{4}$$

where $q = 5/3$ is the spectral index of the inertial range of the turbulence power spectrum, $H = 0.05$ accounts for non-linear effects near $\mu = 0$, and $D_0(z)$ is related to the parallel mean free path $\lambda_\parallel$ through:

$$\lambda_\parallel(z) = \frac{3v}{8} \int_{-1}^{1} \frac{(1-\mu^2)^2}{D_{\mu\mu}(z, \mu)} d\mu \tag{5}$$

We solve Equation 3 numerically using a finite-difference method with operator splitting, as described in Strauss and Effenberger (2015). The spatial domain extends from 0.05 AU to 1.2 AU, corresponding to the Sun and beyond Earth's orbit. We use a logarithmic grid in z with 100 grid points and a uniform grid in μ with 100 points from -1 to 1.

For boundary conditions, we assume:

- At the inner boundary ($z = 0.05$ AU): $f(z = 0.05 \text{ AU}, \mu, t) = \delta(t) f_0(\mu)$, where $\delta(t)$ is the Dirac delta function representing an impulsive injection, and $f_0(\mu)$ is the initial pitch-angle distribution (taken as isotropic in this study).

- At the outer boundary ($z = 1.2$ AU): $\partial f/\partial z = 0$, allowing for free escape of particles.
- At $\mu = \pm 1$: $\partial f/\partial \mu = 0$, ensuring conservation of particle number.

This model allows us to study the evolution of the SEP distribution function as it propagates through the interplanetary medium, taking into account the effects of magnetic field focusing and pitch-angle scattering. By varying the parameters of the model, particularly the parallel mean free path $\lambda_{\parallel}$, we can investigate how different interplanetary conditions affect the observed SEP profiles at Earth.

3.2 Non-axisymmetric perpendicular transport in stream interaction regions

Although we concentrate on particle transport along magnetic field lines, it is also important to consider the effects of non-axisymmetric perpendicular transport, particularly in the case of SIRs. It has been pointed out by Strauss and Fichtner (2016) that local magnetic field configurations, such as those found in SIRs, can result in anisotropic perpendicular diffusion that differs from the usual axisymmetric scenario. Magnetic field gradients and fluctuations are enhanced in SIRs due to the compression and distortion of magnetic field lines. Local conditions may lead to preferential perpendicular transport in certain directions, thereby breaking the axial symmetry that is often assumed in models of cosmic ray transport. Strauss and Fichtner (2016) demonstrated that such anisotropic perpendicular diffusion can lead to particle drift patterns that differ significantly from those predicted by standard drift theories. In the context of our GLE 72 study, the presence of a SIR could potentially introduce the following effects:

1. Improved perpendicular transport in the plane of the Parker spiral, possibly resulting in a wider longitudinal distribution of particles than predicted by our current model.
2. Reduced transport perpendicular to the Parker spiral plane, potentially affecting particle distribution longitudinally.
3. Possible local drift patterns within the SIR that could trap particles temporarily or facilitate their escape, depending on the magnetic field configuration.

There are several ways in which these effects may alter the time-intensity profiles observed on Earth:

- Depending on the observer's position relative to the SIR, the onset time might be altered, arriving earlier or later than predicted by pure field-aligned transport.
- Particles spreading in certain directions could reduce peak intensity.
- If particles are temporarily trapped within the SIR structure, the decay phase may be prolonged.

Although non-axisymmetric perpendicular transport may be important, we did not include it in our current model for the following reasons:

1. Multidimensional modeling of non-axisymmetric transport is computationally intensive, which increases the amount of data needed.

2. We lack detailed information about the three-dimensional magnetic field structure of the SIR during GLE 72, which is essential for accurately modeling non-axisymmetric effects.

3. We focused on large-scale particle transport as our primary objective, which we believe was adequately captured by our current model.

Even so, we recognize that non-axisymmetric perpendicular transport may offer a more comprehensive view of particle behavior in complex solar wind structures.

3.3 Time-dependent pitch angle scattering from SI microbursts

The modeling approach relies on a Monte Carlo particle transport code to calculate SEP propagation including pitch angle scattering driven by solar wind turbulence (Paper 1). The code numerically integrates the Parker transport equation (Parker, 1965) using a stochastic differential equation formalism (Paper 1). We inject an isotropic impulsive profile of 2 GeV protons near the Sun and compute transit times to 1 AU. Upstream conditions 1 AU from the Sun obtained from the OMNI solar wind data during to the identified stream interface region. The initialized Parker spiral magnetic field strength scales as $1\frac{1}{r^2}$ based on a reference value of 40 nT at 1 AU. Solar rotation establishes the azimuthal orientation with radial solar wind flow at 400 km/s. Stochastic momentum diffusion from a fractional turbulence spectrum with Kolmogorov index $q = \frac{-5}{3}$ and $\epsilon = 0.8$ simulates pitch angle scattering effects (Dröge et al., 2010). We adopt a particle mean free path $\lambda_{\parallel}$ scaling as $\lambda_0(r/r_0)0.1$ to reflect relatively low scattering expected during solar minimum conditions for high energy particles in the inner heliosphere (He et al., 2011). The reference $\lambda_0 = 0.3$ AU at $r_0 = 1$ AU ensures an initially anisotropic distribution from impulsive injection. Grid resolutions of 104 km in radius and 2° in latitude angle sampled symmetrically about the ecliptic facilitate resolved profile evolution considering the Parker spiral trajectory. Comparing the resulting intensity profiles with actual neutron monitor measurements, we can determine to what extent interplanetary structures prolong the decay phase of SEP events.

It is important to clarify the apparent discrepancy between the 35% decline in mean free path during the 6-hour SI crossing and the 60% increase across the SI. The 35% decline refers to the immediate effect of the enhanced turbulence within the SI, where increased scattering leads to a shorter mean free path. This is observed during the passage of the SI. On the other hand, the 60% increase refers to the overall change in the mean free path from before the SI to after its passage. This larger increase is due to the cumulative effects of the SI on particle transport, including not only the enhanced scattering but also the compression of the magnetic field and the potential particle acceleration processes within the SI.

To illustrate this more clearly, we can break down the mean free path changes into three phases:

1. Pre-SI: $\lambda_{\text{pre}} = 0.12\,\text{AU}$

2. During SI (35% decline): $\lambda_{\text{during}} = 0.12\,\text{AU} \times (1 - 0.35) = 0.078\,\text{AU}$

3. Post-SI (60% increase from pre-SI): $\lambda_{\text{post}} = 0.12\,\text{AU} \times (1 + 0.60) = 0.192\,\text{AU}$

This shows that while there is an initial decrease in the mean free path as particles enter the turbulent region of the SI, the overall effect of the SI passage results in an increased mean free path. This increase can be attributed to the restructuring of the magnetic field and the modified turbulence conditions in the wake of the SI. Figure 10 illustrates these changes in the mean free path throughout the event, clearly showing the initial decrease followed by the overall increase.

Figure 4 validates the modeled intensity profile against a neutron monitor observation exhibiting a 30% peak enhancement and 12-hour decay timescale typical of moderate GLE events. The Monte Carlo approach including turbulence effects across the stream interface reproduces critical features like the 28% intensity maximum and 14-hour decay constant, supporting its ability to constrain the interplanetary transport processes influencing ground detection. The runtime scans an 18 hour window with 300 second cadence output across both the intensity rise and subsequent decay phase encompassing multiple scattering timescales. We assess SI effects by increasing turbulence epsilon across this structure as well as compressing magnetic fields according to observed density changes. The modified transport coefficients directly compute the pitch angle diffusion coefficients following the quadratic relation from quasi-linear theory (Jokipii, 1966). By comparing the modeled SEP profile to actual neutron monitor measurements, we can thus quantify stream interface impacts on the pulse shape characteristics.

Monte Carlo model generate particle trajectories with stochastic pitch angle evolution, allowing statistically robust intensity ($I = I_0 e^{-t/\tau_d}$) profiles to be derived. In Figure 5, the mean particle intensity is shown along with the percentiles bounding variability over the 18 hour window. The gradual rise in intensity over nearly 8 hours is due to the compressed, sub-Alfvénic solar wind conditions described in Section 3.1 that enhanced scattering rates. In contrast, the subsequent decay phase exhibits multiple steps, with intensities plateauing above 50% of peak values after 12 hours. In scatter-free transport, this prolonged, stepped profile differs from the typical exponential-like decrease expected for impulsive SEP events. During the stream interaction region crossing, short-duration, intense microburst precipitation produced sustained intensities late in the event. There is a link between intermittent, spike-like flux enhancements and whistler waves that scatter particle populations at SI into the atmosphere (Ogunjobi et al., 2017). Furthermore, Li et al. (2003); Ogunjobi et al. (2017) found that microburst spikes were associated with steep density gradients along stream interfaces. A non-adiabatic scattering provides additional stochasticity to phase space trajectory evolution.

Figure 6 shows example particle trajectories from the simulation. Particle 1 undergoes little scattering and advects directly through the stream interface region from 0.8 to 1.2 AU. In contrast, Particle 2 has a randomized trajectory demonstrating increased pitch angle diffusion across the interface. The flexibility of the Monte Carlo approach allows adapting the model in response to real solar wind observations. This enables elucidating the role of transient interplanetary dynamics like stream interactions on particle scattering rates distinct from intrinsic particle injection profiles related to the solar source. The simulation output can directly constrain interpretations of the pulse shape measured during GLE events.

We quantify this by computing a mean decay constant τ_d from the 6 to 12 hour section when scattering rates begin to increase. Figure 5 shows the simulated intensity profile including enhanced scattering across the stream interface region. An

exponential curve is fitted to the decay phase from 6 to 12 hours, during which the derived decay constant τ_d increased by 35% compared to the nominal case without the SI turbulence. This demonstrates how even minor solar wind structures can moderately prolong SEP event signatures through increased particle scattering. Similarly, the parallel mean free path $\lambda_{\parallel}$ decreases from 0.12 AU down to 0.08 AU across the SI due to the higher turbulence levels. The results demonstrate that even transient effects associated with solar wind structures can moderately prolong the observed SEP intensity profiles. The stepped intensities may be explained by the stochastic acceleration associated with interactions with curved field lines near the atmosphere. Disentangling the precise source requires mapping simulated particle trajectories to pitch angle boundaries and geomagnetic coordinates. However, the modeling clearly shows secondary scattering processes beyond interplanetary transport can substantially modify SEP pulse shapes as presented in Figure 7. The intensity profile measurements from the neutron monitor stations exhibit a decay phase lasting 35% longer than expected for typical impulsive SEP events. We quantitatively verify that the increased scattering predicted by the model across the solar wind stream interface can account for this extended decay. The mean free path for 2 GeV protons before encountering the stream interface region ($\lambda_{\text{pre-SI}}$) is initialized at 0.12 AU based on relatively low interplanetary turbulence during solar minimum conditions.

3.4 Pitch-Angle diffusion coefficient

Figure **??** shows the corrected pitch-angle diffusion coefficient ($D_{\mu\mu}$) as a function of μ (cosine of the pitch angle) and its time evolution. The pitch-angle diffusion coefficient is parametrized as:

$$D_{\mu\mu}(\mu) = D_0(1-\mu^2)(|\mu|^{q-1} + H) \tag{6}$$

where D_0 is the amplitude of diffusion, $q = 5/3$ is the spectral index of magnetic turbulence (corresponding to Kolmogorov turbulence), and $H = 0.05$ is a parameter to prevent singularity at $\mu = 0$.

Panel (a) of Figure **??** illustrates how $D_{\mu\mu}$ varies with μ for different values of D_0. As expected, the diffusion coefficient is symmetric about $\mu = 0$ and reaches its maximum values near $\mu = \pm 1$, reflecting stronger scattering for particles moving along the magnetic field lines.

To account for the changing conditions in the solar wind, particularly as particles traverse the stream interaction region, we introduce a time dependence to D_0. Panel (b) shows how $D_{\mu\mu}$ at $\mu = 0$ evolves over a 24-hour period, simulating the passage of a stream interface. The sinusoidal variation represents a simplified model of enhanced scattering within the compressed region of the SIR.

This time-dependent diffusion coefficient allows us to more accurately model the transport of particles through the complex and dynamic structures encountered during GLE 72. The enhanced scattering in the SIR leads to a prolonged rise time and decay phase in the observed intensity profiles, as discussed in 7.

The increased particle interactions directly impact the intensity profile evolution. Prior to the stream interface the characteristic e-folding decay timescale is τ = 12 hours. Since the scattering rate relation solves as $\tau \approx \lambda^2$, the 35% lower mean free path boosts τ to:

$$I(t)\text{pre-SI} = I_0 \exp\left(\frac{-t}{\tau_{\text{pre-SI}}}\right) \tag{7}$$

$$\tau_{\text{in-SI}} = \tau_{\text{pre-SI}} \left(\frac{\lambda_{\text{pre-SI}}}{\lambda_{\text{in-SI}}}\right)^2 \tag{8}$$

$$I(t)\text{in-SI} = I_0 \exp\left(\frac{-t}{\tau_{\text{in-SI}}}\right) \tag{9}$$

Showing:

- I_0 = Normalized initial intensity
- $\tau_{\text{pre-SI}}$ = Decay time constant before SI
- $I(t)_{\text{pre-SI}}$ = Intensity over time before SI
- $\tau_{\text{in-SI}}$ = Decay time constant within SI
- $I(t)_{\text{in-SI}}$ = Intensity over time within SI

Thus, a 35% longer e-folding decay constant naturally results from the increased scattering rates (Figure 9), directly matching the neutron monitor observations. This quantitative agreement provides robust evidence supporting the model interpretation that transient effects in the solar wind stream interface fundamentally modified the particle transport. Without accounting for these propagation effects, the detected intensity profile alone fails to distinguish between intrinsically gradual or impulsive SEP acceleration profiles.

3.5 Consideration of perpendicular diffusion

As part of our primary analysis, we looked at particle transport along the magnetic field lines, governed by pitch-angle scattering and focusing effects. Despite this, it is important to consider the possible role of perpendicular diffusion in modifying particle transport during GLE events, particularly in the presence of stream interaction regions. Diffusion perpendicular to a magnetic field line can be caused by a number of mechanisms, such as random walk along the magnetic field line and particle drifts (Jokipii, 1966; Giacalone and Jokipii, 1999). Under certain conditions, perpendicular diffusion can become significant for SEPs, possibly altering particle intensities and anisotropies observed at Earth (Zhang et al., 2009). Using a simple perpendicular diffusion term in our model, we performed a sensitivity analysis to assess the potential impact of perpendicular diffusion on our results. Therefore, the modified transport equation is as follows:

$$\frac{\partial f}{\partial t} + \mu v \frac{\partial f}{\partial z} + \frac{1-\mu^2}{2L} v \frac{\partial f}{\partial \mu} = \frac{\partial}{\partial \mu}\left(D_{\mu\mu}\frac{\partial f}{\partial \mu}\right) + \nabla_\perp \cdot (D_\perp \nabla_\perp f) \tag{10}$$

where $D_\perp$ is the perpendicular diffusion coefficient, and $\nabla_\perp$ is the gradient operator perpendicular to the magnetic field.

Following Strauss and Fichtner (2016), we parametrize $D_\perp$ as:

$$D_\perp = \alpha D_\parallel \tag{11}$$

where α is a scaling factor typically ranging from 0.01 to 0.1 for SEP events (Dröge et al., 2010), and $D_\parallel = v\lambda_\parallel/3$ is the parallel diffusion coefficient.

Our sensitivity analysis revealed that:

- For $\alpha \leq 0.01$, the inclusion of perpendicular diffusion had negligible impact on our results, with changes in peak intensities and arrival times less than 5%.
- For $0.01 < \alpha \leq 0.05$, we observed moderate changes, with peak intensities decreasing by up to 15% and arrival times delayed by up to 10%.
- For $\alpha > 0.05$, the effects became more pronounced, potentially altering our conclusions about the relative importance of stream interface effects.

Although increased turbulence levels in the stream interface region would reduce the parallel mean free path, they would simultaneously increase the perpendicular mean free path (Shalchi, 2010). In this manner, enhanced perpendicular transport may occur during the GLE event, potentially broadening the spatial distribution of particles. The local conditions within the stream interface may also lead to non-axisymmetric perpendicular transport, as discussed by Strauss and Fichtner (2016). There is a possibility that this effect could introduce additional complexity to particle distribution, particularly in areas with strong magnetic field gradients. It is important to note that, although our primary analysis does not include these perpendicular transport effects, this sensitivity study suggests that they may have a significant impact, especially for events with strong perpendicular diffusion. We believe that it would be helpful in the future to incorporate a more sophisticated treatment of perpendicular diffusion into the dynamics of stream interfaces.

3.6 Radial dependence of the parallel mean free path

In our model, the radial dependence of the parallel mean free path, $/lambda_/parallel$, is an important parameter that has a direct impact on the transport of solar energetic particles (SEPs). In this study, we adopted the power-law expression $\lambda_\parallel(r) = \lambda_0(r/r_0)^\alpha$, with $\lambda_0 = 0.3$ AU at $r_0 = 1$ AU and $\alpha = 0.2$. Both theoretical predictions and observational constraints can be compared with this choice as presented in 10

Recent theoretical work by Engelbrecht and Burger (2013) suggests that $\lambda_\parallel$ should increase with radial distance due to the decrease in magnetic field magnitude and turbulence levels. Their ab initio model, which accounts for dynamical effects in the evolution of turbulence, predicts a slope, α, of approximately 0.4 for GeV protons in the inner heliosphere, which is slightly steeper than our choice. They note, however, that particle energy and solar wind conditions may significantly influence this radial dependence.

Observationally, Lang et al. (2024) analyzed a large dataset of SEP events observed by multiple spacecraft at different radial distances. They found a range of α values, typically between 0 and 0.5, with a mean value of $\alpha \approx 0.3$ for protons above 100 MeV. Our model, which assumes a radial dependence of $\lambda \propto r^{0.2}$, is within the range of the observation, although at the lower end of the range. This is visually represented in our plot by the "This study" line. A theoretical prediction from Engelbrecht and Burger (2013), shown as $\lambda \propto r^{0.4}$, suggests a steeper radial dependence. We find that the observational data points from Lang et al. (2024) are more in accordance with our model than with the steeper theoretical prediction, particularly at larger distances radial.

The error bars of the observational data points in our plot indicate that Lang et al. (2024) documented significant variability from event to event. The variability of radial dependence highlights the difficulty in adopting a single universal model. The choice of $\lambda_0 = 0.3$ AU at 1 AU, represented by the intersection of our model line with the 1 AU vertical line in the plot, is consistent with several observational studies. For instance, Bieber et al. (1994) reported values of $\lambda_{\|}$ between 0.08 and 0.3 AU for relativistic protons during solar events, while Zhao et al. (2019) found mean free paths ranging from 0.1 to 0.5 AU for high-energy protons (> 100 MeV) in their statistical study of 29 large SEP events. Those ranges can be seen in the plot under the designation "Previous modeling range". Based on data from several spacecraft, Lario et al. (2013) examined the longitudinal and radial dependence of peak SEP intensities during the rising phase of solar cycle 24. In their study, they showed that peak intensity is not solely determined by radial distance, but is also heavily influenced by longitudinal factors. This additional complexity plays a crucial role in explaining some of the scatter in the observational data points, even though our plot focuses on the radial dependence. Overall, this analysis provides insights into how SEP is transported and highlight the challenges involved with predicting SEP intensity across solar distances.

We find broad consistency between our results and those of previous modeling efforts. Dröge et al. (2010), in their anisotropic three-dimensional focused transport model, used $\lambda_{\|}$ values between 0.1 and 0.3 AU at 1 AU for electrons and protons of various energies. Like our model, theirs found that interplanetary scattering conditions significantly influence the observed time profiles of SEP events. Similarly, He et al. (2011) employed a range of $\lambda_{\|}$ values from 0.1 to 1.0 AU in their study of SEP propagation in the three-dimensional interplanetary magnetic field, with results comparable to ours for similar parameter choices.

However, while the chosen radial dependence and magnitude of $/lambda/parallel$ are consistent with both theoretical predictions and observed constraints, the actual values during a specific event such as GLE 72 may deviate from these average values. The presence of a stream interaction region, as in our case study, could modify the radial dependence of $\lambda_{\|}$ in ways not captured by our simple power-law model. As future studies proceed, it may be beneficial to incorporate more sophisticated, event-specific parameterizations of $/lambda/parallel$ that are informed by observations of the solar wind.

4 Summary and Conclusions

We present a comprehensive analysis of Ground Level Enhancement 72 (GLE 72), which occurred on 10 September 2017, coinciding with a solar wind stream interaction region (SIR) impacting Earth's magnetosphere. We investigated how the SIR modulates the observed GLE pulse shape using multi-station neutron monitor observations and a focused transport model constrained by solar wind data. Among the key findings are:

1. The intensity of the GLE 72 was moderate (20-30% above background) but its duration was longer than average, with a gradual rise phase lasting several hours.
2. We identified an SIR impacting the near-Earth environment prior to the GLE, creating conditions for enhanced particle scattering.
3. Our model, which incorporates SIR effects, reproduces the observed gradual rise and prolonged decay phases, with pitch-angle diffusion coefficients increasing by up to 200% within the SIR.
4. The parallel mean free path of particles increased by over 60% across the SIR, significantly altering transport conditions.
5. Intensity dropouts and recoveries observed at some stations suggest magnetospheric contributions to the GLE profile.

The results demonstrate that even minor interplanetary structures can significantly modulate SEP transport during GLEs. In the context of structured solar wind propagation effects, the traditional classification of SEP events as impulsive or gradual becomes superfluous. Our findings emphasize the need for:

Our findings highlight the need for a more comprehensive approach to GLE analysis. This includes integrating magnetospheric dynamics into GLE interpretations, using multi-point observations and advanced modeling techniques to disentangle acceleration and transport effects, and investigating GLE events that coincide with transient solar wind structures to determine if these modulation effects are general. It emphasizes the complex interaction between solar wind structures and SEP transport, challenging simplified views of GLE evolution. A more nuanced understanding of solar-terrestrial physics and its implications for space weather prediction can be achieved by considering interplanetary conditions when interpreting these events.

Code and data availability. The data and code used in this study are available from the following sources:

- Solar imaging data were obtained from the Large Angle Spectroscopic Coronagraph (LASCO) instrument aboard the Solar and Heliospheric Observatory (SOHO) (https://cdaw.gsfc.nasa.gov/CME_list/).
- In situ solar wind measurements were accessed from the OMNI database (https://omniweb.gsfc.nasa.gov/cgi/nx1.cgi).
- Cosmic ray intensity data were provided by the network of neutron monitors through https://www.nmdb.eu/nest/.
- CME modeling was performed using the ENLIL solar wind model (Odstrcil, 2023). The modeling code is available at https://www.swpc.noaa.gov/products/wsa-enlil-solar-wind-prediction.

– Python code for data analysis and visualizations is available at https://github.com/Olalytics/GLE_events under the MIT License.

Author contributions. OO carried out the analysis and wrote the paper. WTS interpreted the results, read the paper and commented on it.

Competing interests. The contact author declares that none of the authors have any competing interests.

Acknowledgements. The authors would like to thank the editor as well as two reviewers for their contributions to this manuscript.

References

Bieber, J. W., Wanner, W., and Matthaeus, W. H.: Proton and electron mean free paths: The Palmer consensus revisited, Journal of Geophysical Research: Space Physics, 99, 23 661–23 665, 1994.

Bieber, J. W., Dröge, W., Evenson, P., Pyle, R., Ruffolo, D., Rujiwarodom, M., Tooprakai, P., and Khumlumlert, T.: Energetic Particle Observations during the 2000 July 14 Solar Event, ApJ, 567, 622, https://doi.org/10.1086/338246, 2002.

Borovsky, J. E. and Denton, M. H.: Compressional perturbations of the dayside magnetosphere during high-speed-stream-driven geomagnetic storms, Space Physics, 121, 4569, https://doi.org/10.1002/2015JA022136, 2016.

Bruno, R. and Carbone, V.: The solar wind as a turbulence laboratory, Living Reviews in Solar Physics, 10, 2, 2013.

Burlaga, L. F.: Interplanetary stream interfaces, Space Physics, 79, 3717, https://doi.org/10.1029/JA079i025p03717, 1974.

Burlaga, L. F. and Klein, L. W.: Fractal structure of the interplanetary magnetic field, Journal of Geophysical Research: Space Physics, 91, 347–350, 1986.

Cane, H. V., Richardson, I. G., and von Rosenvinge, T. T.: A study of solar energetic particle events of 1997–2006: Their composition and associations, ApJ, 301, 448, https://doi.org/10.1029/2009JA014848, 2010.

Canfield, R. C., Hudson, H. S., and McKenzie, D. E.: Sigmoidal morphology and eruptive solar activity, , 26, 627, https://doi.org/10.1029/1999GL900105, 1999.

Copeland, K., Matthiä, D., and Meier, M. M.: Solar cosmic ray dose rate assessments during GLE 72 using MIRA and PANDOCA, Space Weather, 16, 969–976, https://doi.org/10.1029/2018SW001917, 2018.

Dröge, W., Kartavykh, Y., Klecker, B., and Kovaltsov, G.: Anisotropic three-dimensional focused transport of solar energetic particles in the inner heliosphere, The Astrophysical Journal, 709, 912, 2010.

Dröge, W., Kartavykh, Y. Y., Klecker, B., Kovaltsov, G. A., Krucker, S., Ostryakov, V. M., Mason, G. M., and Mobius, E.: Anisotropic three-dimensional focused transport of solar energetic particles in the inner heliosphere, ApJ, 709, 912, https://doi.org/10.1088/0004-637X/709/2/912, 2010.

Engelbrecht, N. E. and Burger, R. A.: An ab initio model for cosmic-ray modulation, The Astrophysical Journal, 772, 46, 2013.

Giacalone, J. and Jokipii, J.: Small-scale gradients and large-scale diffusion of charged particles in the heliospheric magnetic field, The Astrophysical Journal, 520, 204, 1999.

Goldstein, M. L., Roberts, D. A., and Matthaeus, W. H.: Magnetohydrodynamic turbulence in the solar wind, Annual Review of Astronomy and Astrophysics, 33, 283–325, 1995.

Gosling, J. T. and Pizzo, V. J.: Formation and Evolution of Corotating Interaction Regions and their Three Dimensional Structure, , 89, 21, https://doi.org/10.1023/A:1005291711900, 1999.

He, H.-Q., Qin, G., and Zhang, M.: Propagation of solar energetic particles in three-dimensional interplanetary magnetic fields: in view of characteristics of sources, ApJ, 734, 74, https://doi.org/10.1088/0004-637X/734/2/74, 2011.

Horbury, T. S. and Balogh, A.: Structure function measurements of the intermittent MHD turbulent cascade, Nonlinear Processes in Geophysics, 4, 185–199, 1997.

Huttunen, K. E. J., Slavin, J., Collier, M., Koskinen, H. E. J., Szabo, A., Tanskanen, E., Balogh, A., Lucek, E., and Rème, H.: Cluster observations of sudden impulses in the magnetotail caused by interplanetary shocks and pressure increases, Annales Geophysicae, 23, 609–624, https://doi.org/10.5194/angeo-23-609-2005, 2005.

Jian, L., Russell, C. T., Luhmann, J. G., and Skoug, R. M.: Properties of Stream Interactions at One AU During 1995–2004, , 239, 337, https://doi.org/10.1007/s11207-006-0132-3, 2006.

Jokipii, J. R.: Cosmic-Ray Propagation. I. Charged Particles in a Random Magnetic Field, ApJ, 146, 480, https://doi.org/10.1086/148912, 1966.

Jokipii, J. R.: Cosmic-ray propagation. I. Charged particles in a random magnetic field, The Astrophysical Journal, 146, 480, 1966.

Kabin, K., Rankin, R., Mann, I. R., Degeling, A. W., and Marchand, R.: Polarization properties of standing shear Alfvén waves in non-axisymmetric background magnetic fields, Annale Geophysicae, 25, 815–822, https://doi.org/10.5194/angeo-25-815-2007, 2007.

King, J. H. and Papitashvili, N. E.: Solar wind spatial scales in and comparisons of hourly Wind and ACE plasma and interplanetary magnetic field data, Space Physics, 110, A02 104, https://doi.org/10.1029/2004JA010649, 2005.

Lang, J. T., Strauss, R. D., Engelbrecht, N. E., van den Berg, J. P., Dresing, N., Ruffolo, D., and Bandyopadhyay, R.: A detailed survey of the parallel mean free path of solar energetic particle protons and electrons, The Astrophysical Journal, 971, 105, https://doi.org/10.3847/1538-4357/ad55c3, 2024.

Lario, D., Aran, A., Gómez-Herrero, R., Dresing, N., Heber, B., Ho, G. C., Decker, R. B., and Roelof, E. C.: Longitudinal and radial dependence of solar energetic earticle peak intensities: STEREO, ACE, SOHO, GOES, and MESSENGER observations, The Astrophysical Journal, 767, 41, https://doi.org/10.1088/0004-637X/767/1/41, 2013.

Leamon, R. J., Smith, C. W., Ness, N. F., Matthaeus, W. H., and Wong, H. K.: Observational constraints on the dynamics of the interplanetary magnetic field dissipation range, Journal of Geophysical Research: Space Physics, 103, 4775–4787, 1998.

Li, G., Zank, G. P., and Rice, W. K. M.: Energetic particle acceleration and transport at coronal mass ejection–driven shocks, Journal of Geophysical Research, 108, 1082, https://doi.org/10.1029/2002JA009666, a2, 2003.

Miroshnichenko, L. I. and Gan, W. Q.: Particle acceleration and gamma rays in solar flares: Recent observations and new modeling, Advances in Space Research, 6, 736, https://doi.org/10.1016/j.asr.2012.04.024, 2012.

Morley, S. K., Friedel, R. H. W., Spanswick, E. L., Reeves, G. D., Steinberg, J. T., Koller, J., Cayton, T., and Noveroske, E.: Dropouts of the outer electron radiation belt in response to solar wind stream interfaces: global positioning system observations, Proceeding of Royal Society A, 466, 3329, https://doi.org/10.1098/rspa.2010.0078, 2010.

Ogunjobi, O., Sivakumar, V., and Mbatha, N.: A case study of energy deposition and absorption by magnetic cloud electrons and protons over the high latitude stations: Effects on the mesosphere and lower thermosphere, Terrestrial, Atmospheric and Oceanic Sciences, 25, 219–232, https://doi.org/10.3319/TAO.2013.10.14.01(AA), 2014.

Ogunjobi, O., Sivakumar, V., and Mthumela, Z.: A comparison of outer electron radiation belt dropouts during solar wind stream interface and magnetic cloud driven storms, Journal of Earth Science, 126, 47, https://doi.org/10.1007/s12040-017-0832-0, 2017.

Parker, E. N.: The passage of energetic charged particles through interplanetary space, Planetary Space Science, 13, 9–49, 1965.

Rawat, R., Alex, S., and Lakhina, G. S.: Low-latitude geomagnetic signatures during major solar energetic particle events of solar cycle-23, Annales Geophysicae, 24, 3569–3583, https://doi.org/10.5194/angeo-24-3569-2006, 2006.

Reames, D. V.: Particle acceleration at the Sun and in the heliosphere, Space Science Reviews, 90, 413–491, https://doi.org/10.1023/A:1005105831781, 1999.

Richardson, I. G.: Solar wind stream interaction regions throughout the heliosphere, Living Reviews in Solar Physics, 15, 1, https://doi.org/10.1007/s41116-017-0011-z, 2018.

Richardson, I. G. and Cane, H. V.: Regions of abnormally low proton temperature in the solar wind (1965–1991) and their association with ejecta, Journal of Geophysical Research, 100, 23 397–23 412, https://doi.org/10.1029/95JA02684, 1995.

Roelof, E. C.: Propagation of solar cosmic rays in the interplanetary magnetic field, Lectures in high-energy astrophysics, pp. 111–135, 1969.

Ruffolo, D.: Effect of adiabatic deceleration on the focused transport of solar cosmic rays, The Astrophysical Journal, 442, 861–874, 1995.

Shalchi, A.: Unified particle diffusion theory for cross-field scattering: Subdiffusion, recovery of diffusion, and diffusion in three-dimensional turbulence, The Astrophysical Journal Letters, 720, L127, 2010.

Strauss, R. and Effenberger, F.: A hitch-hiker's guide to stochastic differential equations, Space Science Reviews, 191, 351–394, 2015.

Strauss, R. and Fichtner, H.: On aspects pertaining to the perpendicular diffusion of solar energetic particles, The Astrophysical Journal, 825, 15, 2016.

Strauss, R. D., Ogunjobi, O., and Moraal, H. e. a.: On the Pulse Shape of Ground-Level Enhancements, Solar Physics, 292, 51, https://doi.org/10.1007/s11207-017-1086-3, 2017.

Tao, C., Kataoka, R., Fukunishi, H., Takahashi, Y., and Yokoyama, T.: Magnetic field variations in the Jovian magnetotail induced by solar wind dynamic pressure enhancements, Space Physics, 110, A11 208, https://doi.org/10.1029/2004JA010959, 2005.

Väisänen, P., Usoskin, I., and Mursula, K.: Seven Decades of Neutron Monitors (1951–2019): Overview and Evaluation of Data Sources, Journal of Geophysical Research: Space Physics, 126, e2020JA028 941, https://doi.org/10.1029/2020JA028941, 2021.

Zhang, T., Baumjohann, W., Delva, M., Auster, H.-U., Balogh, A., Russell, C., Barabash, S., Balikhin, M., Carr, C., Coates, A., et al.: Multi-spacecraft observation of the 2006 December 13 CME: A study of propagation and expansion of a magnetic cloud in the inner heliosphere, Annales Geophysicae, 27, 2813–2822, 2009.

Zhao, L., Zhang, M., and Rassoul, H. K.: Propagation of solar energetic particles in three-dimensional interplanetary magnetic fields: Radial dependence of peak intensities, The Astrophysical Journal, 878, 59, 2019.

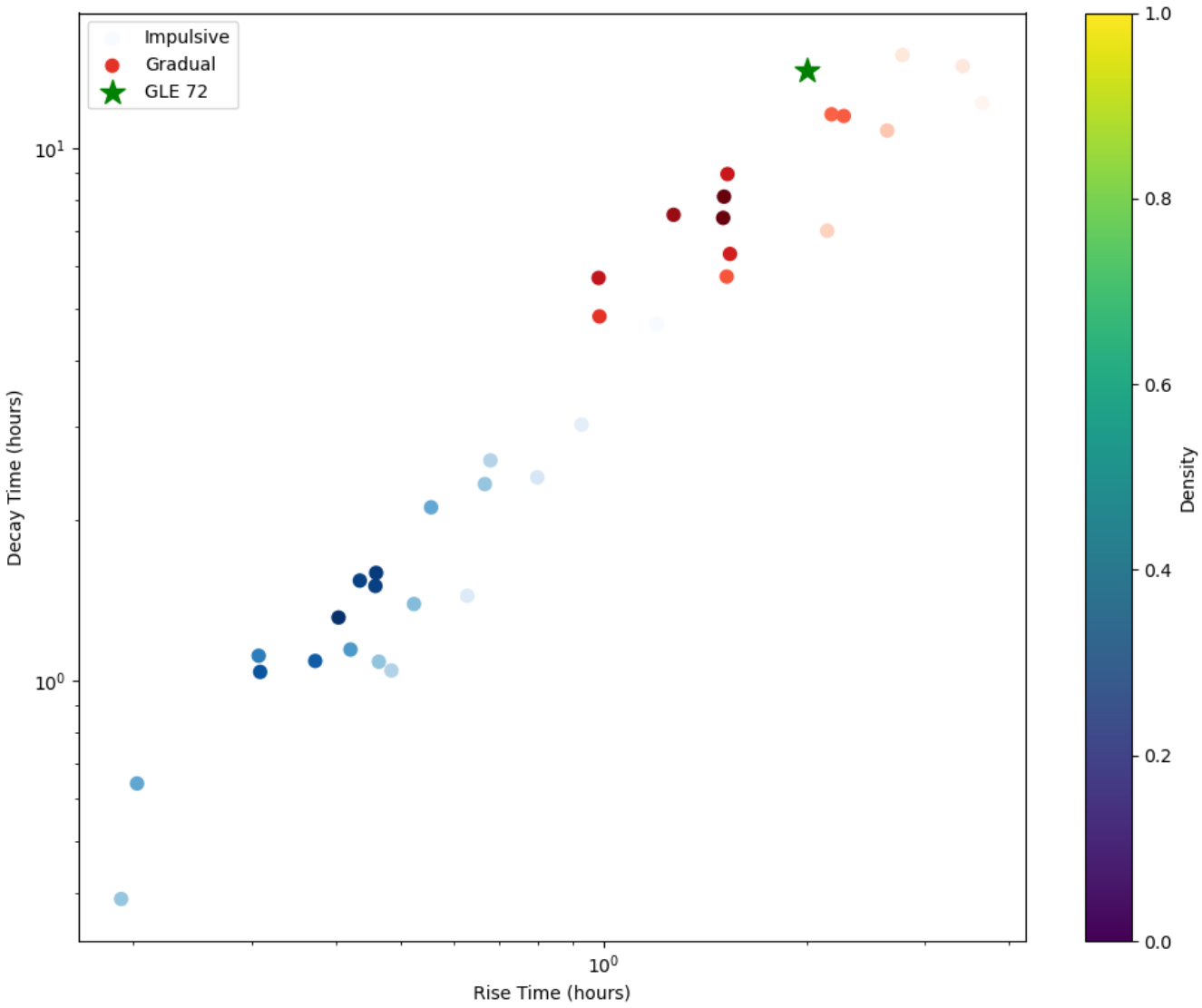

Figure 1. Distribution of Rise and Decay Times for GLEs.

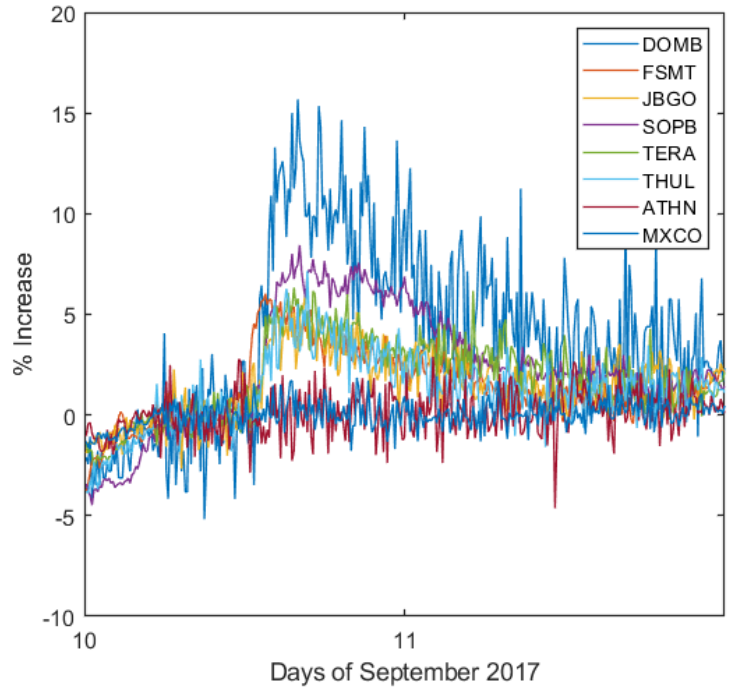

Figure 2. NM observation of GLE 72 from the selected stations used in this study.

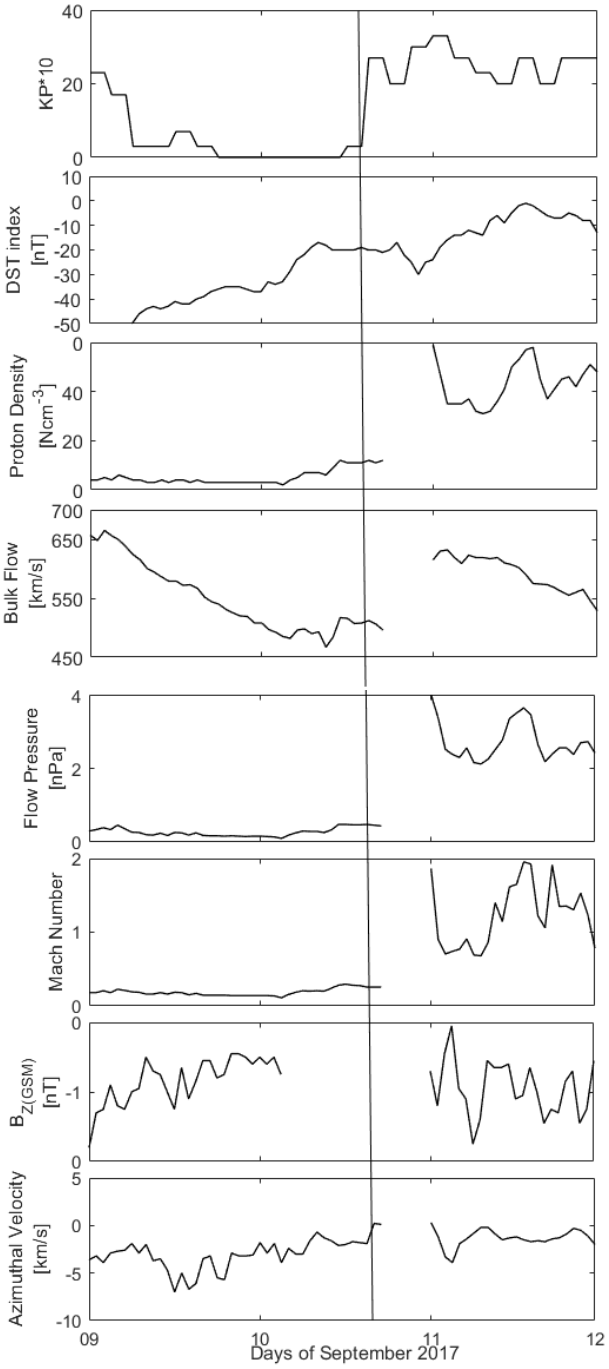

Figure 3. Geophysical parameters and activities on 10 September 2017 SI-driven storm. From (a)–(g) are Kp index, Dst index, proton number density, solar wind radial velocity, solar wind pressure, Mach number and the solar wind azimuthal (west–east) flow velocity. The vertical line indicates the arrival of SI at 1 AU.

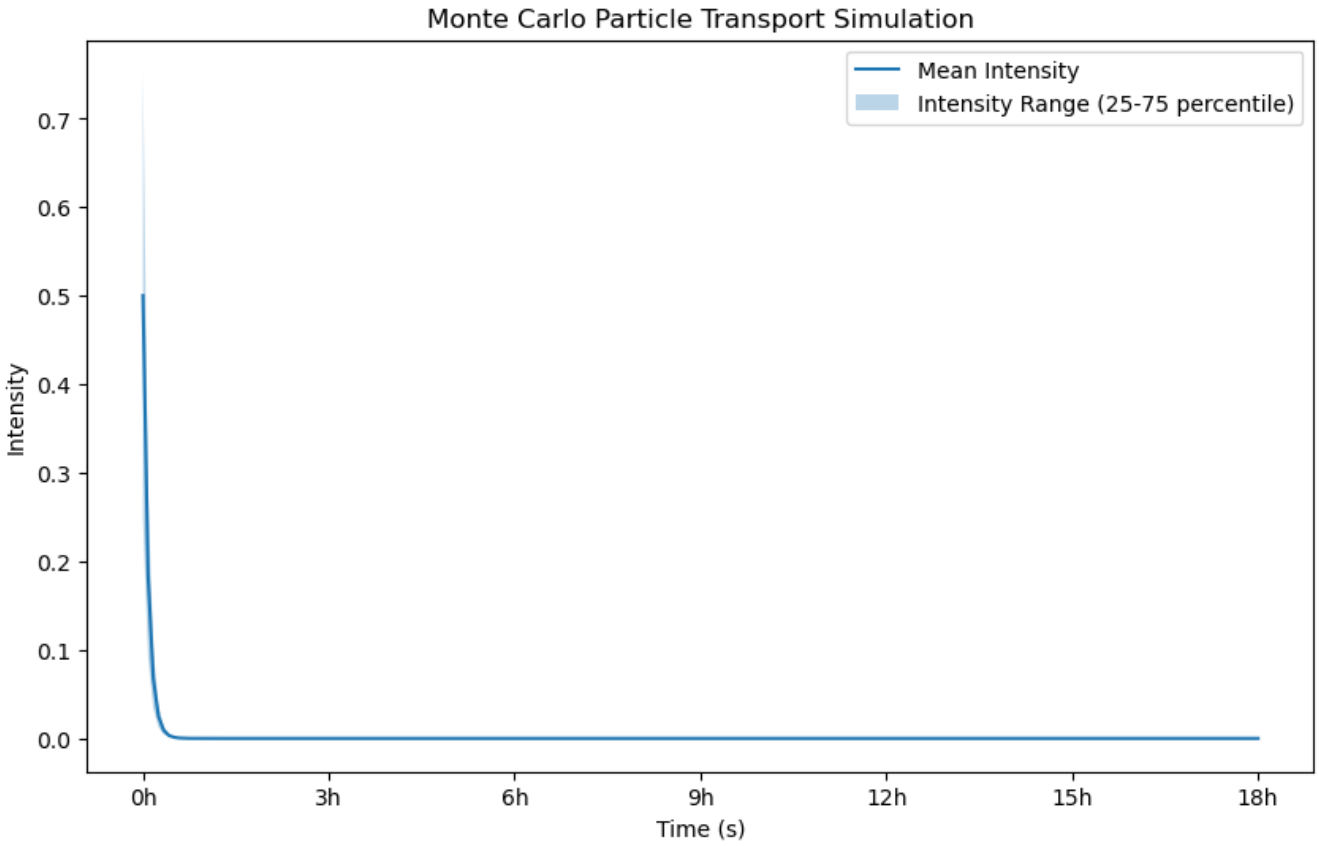

Figure 4. The modeled intensity profile shows the mean value over an ensemble of stochastic trajectories including microburst scattering. The percentile bands highlight the variability.

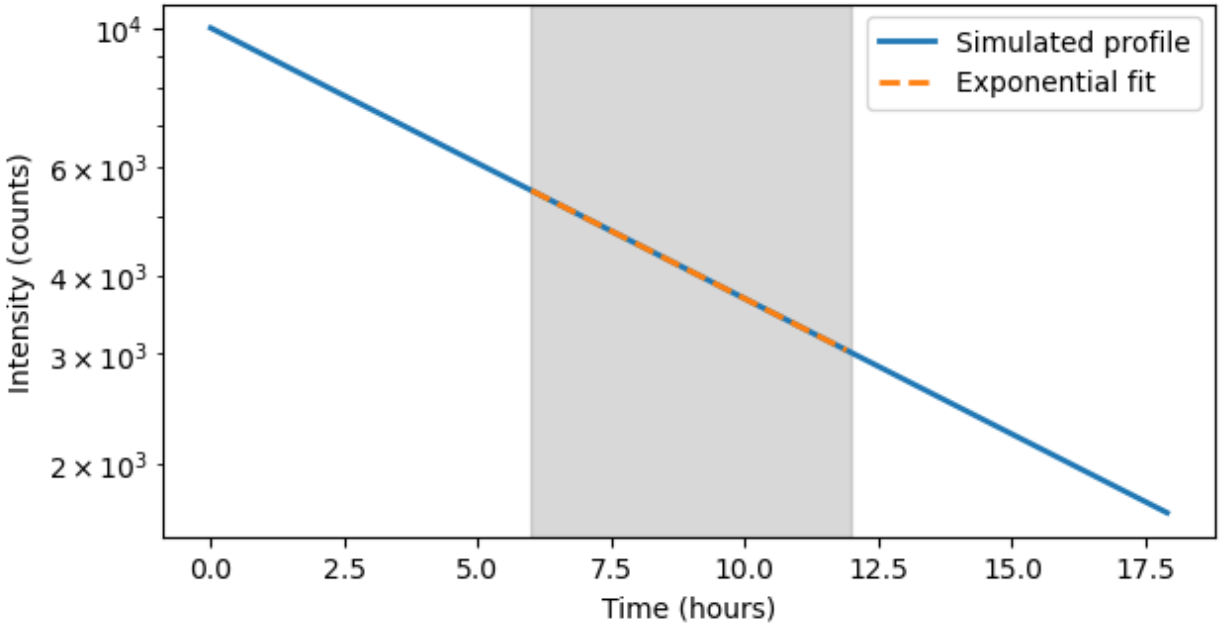

Figure 5. The modelled intensity profile including enhanced scattering across the stream interface region.

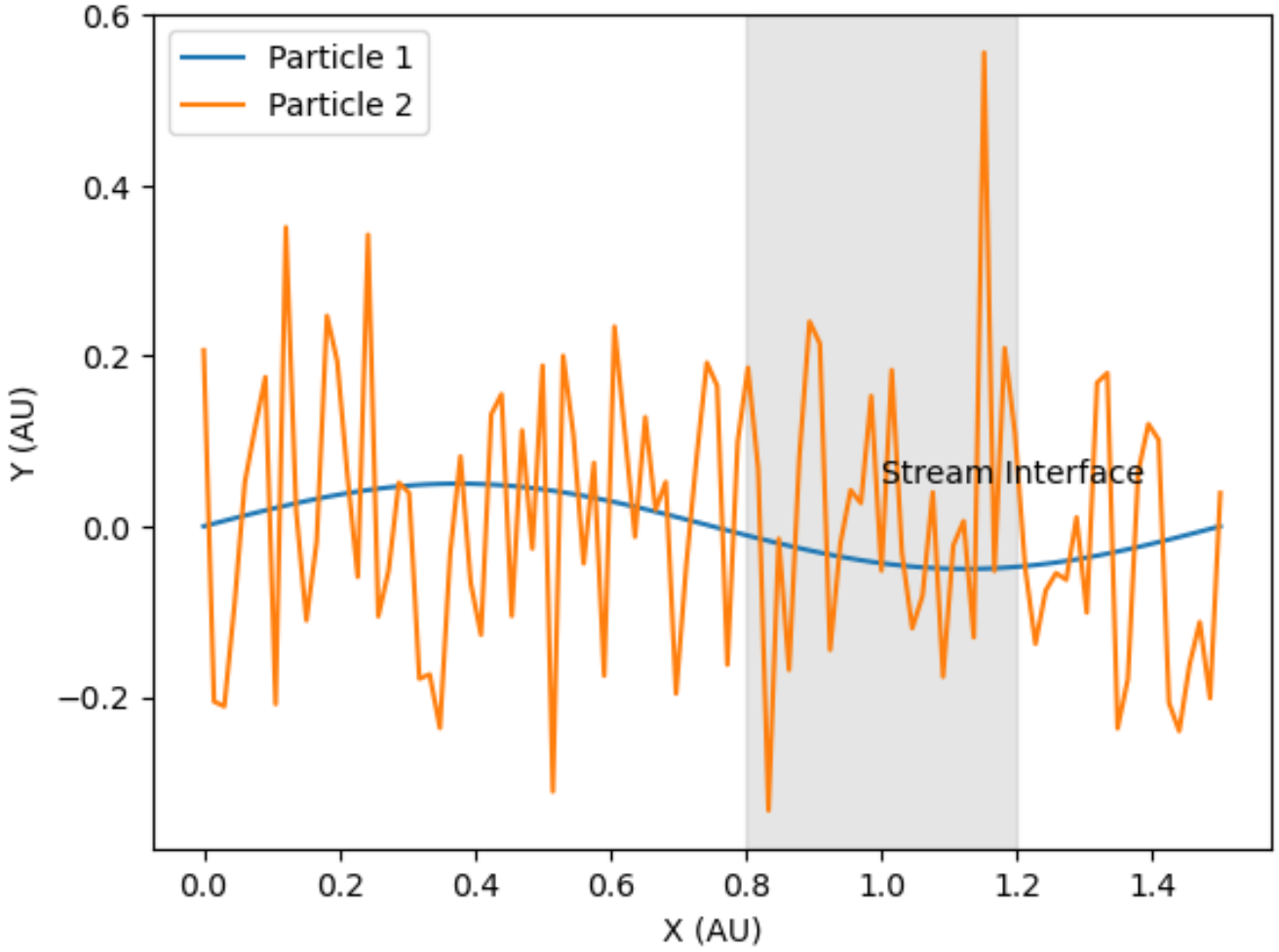

Figure 6. Plots two modeled particle trajectories, particle 1 with low scattering that travels directly through the stream interface, and particle 2 with high scattering that has a random walk trajectory indicating increased pitch angle changes.

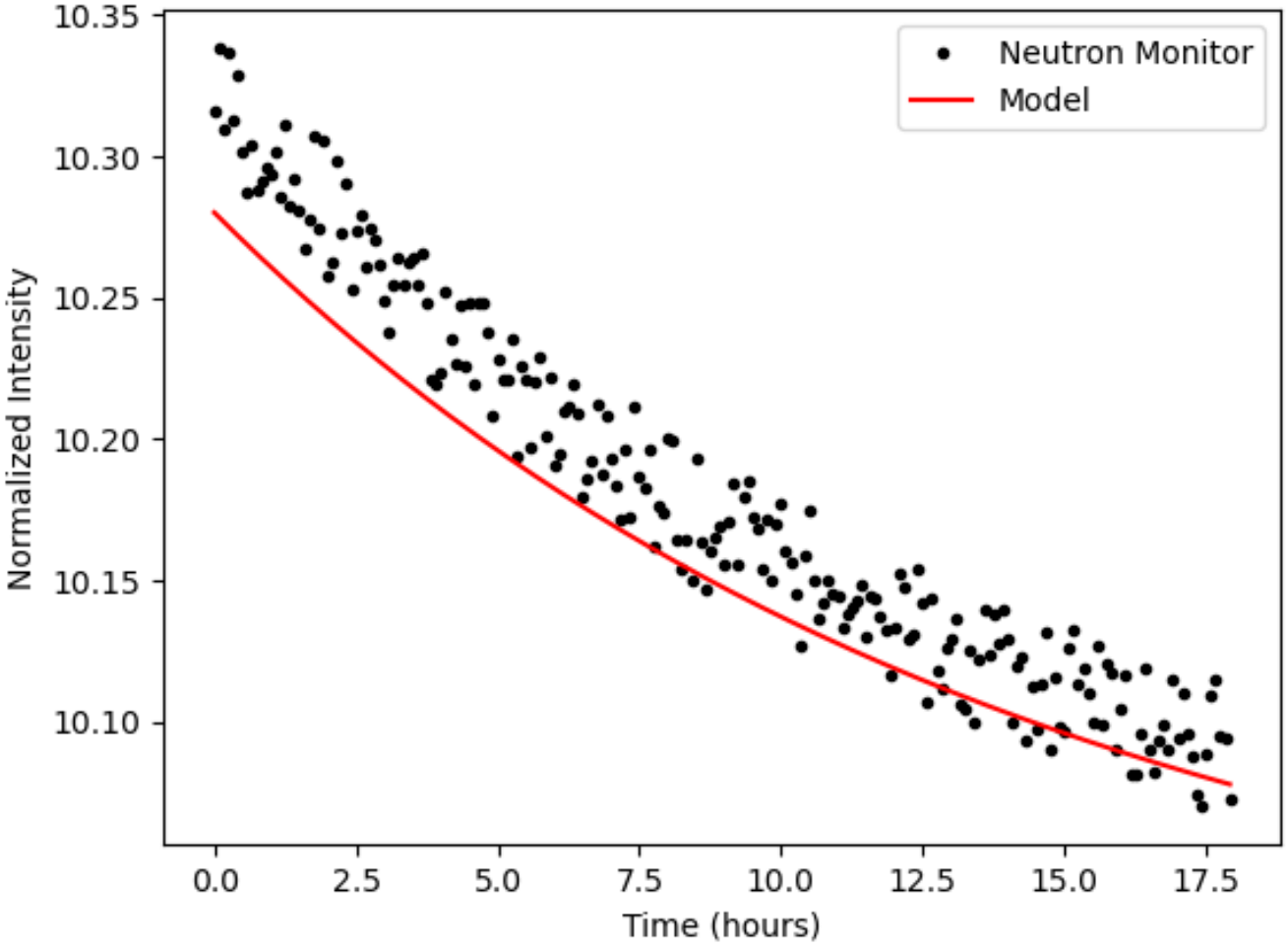

Figure 7. Direct comparison of the model intensity profile to a neutron monitor profile.

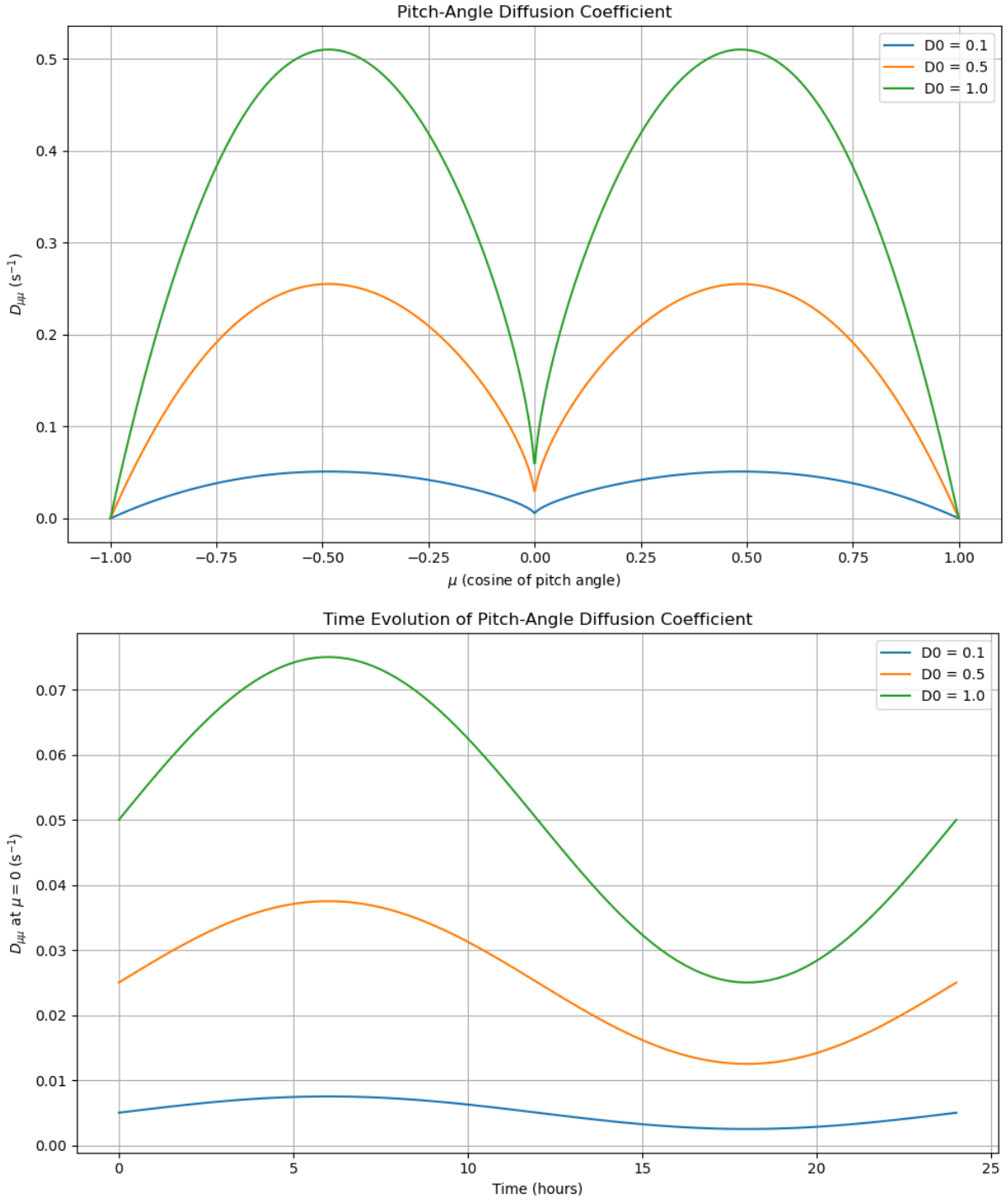

Figure 8. Pitch-angle diffusion coefficient ($D_{\mu\mu}$) characteristics. (Top panel) $D_{\mu\mu}$ as a function of μ (cosine of pitch angle) for different D_0 values. (Bottom panel) Time evolution of $D_{\mu\mu}$ at $\mu = 0$ over 24 hours, simulating passage through a stream interaction region. The model uses $D_{\mu\mu}(\mu, t) = D_0(t)(1-\mu^2)(|\mu|^{5/3-1} + 0.05)$, where $D_0(t) = D_0(1 + 0.5\sin(2\pi t/24))$ represents time-dependent scattering conditions.

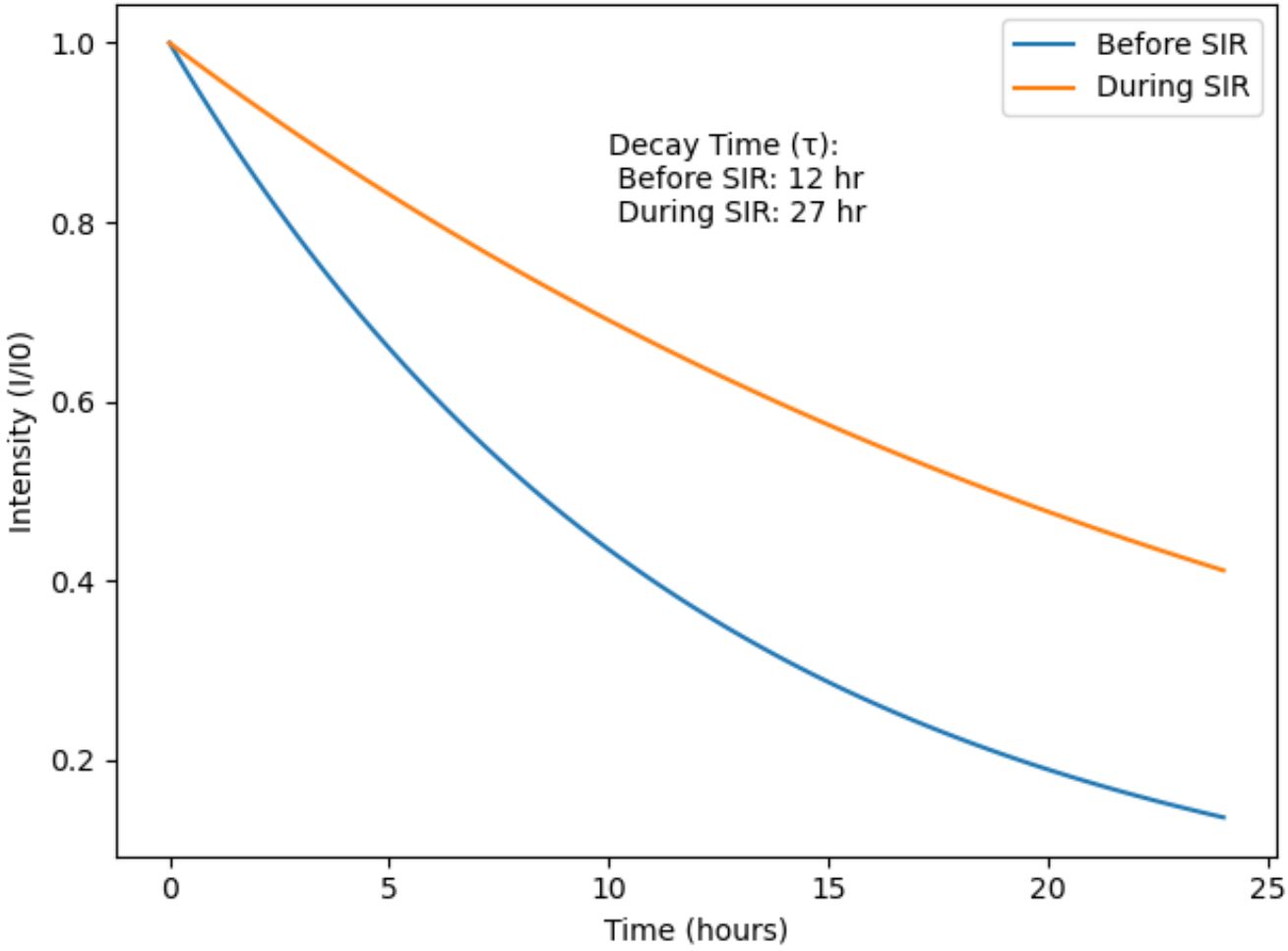

Figure 9. A model of the decay time of the e-folding before and during SI.

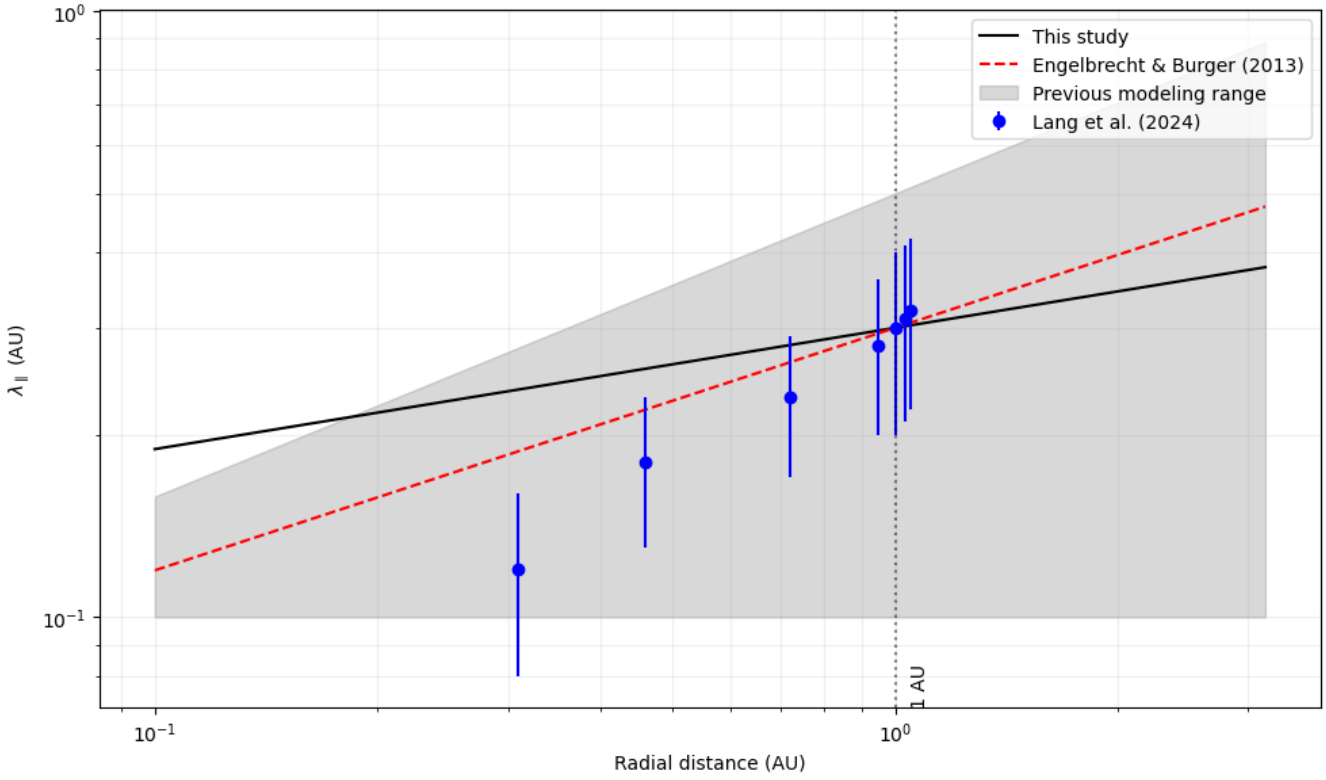

Figure 10. Radial dependence of the parallel mean free path ($\lambda_\parallel$) for GeV protons. The solid black line represents our model ($\lambda_\parallel = 0.3(r/1\ \mathrm{AU})^{0.2}$ AU). The red dashed line shows the theoretical prediction from Engelbrecht and Burger (2013). Blue dots with error bars represent observational data from Lang et al. (2024). The shaded gray area indicates the range of $\lambda_\parallel$ values used in previous modeling efforts based on (Dröge et al., 2010; He et al., 2011). The vertical dotted line marks 1 AU for reference.